ADVANCED FUNCTIONAL MATERIALS
www.afm-journal.de

A Variable Stiffness Magnetic Catheter Made of a Conductive Phase-Change Polymer for Minimally Invasive Surgery

*Yegor Piskarev, Jun Shintake, Christophe Chautems, Jonas Lussi, Quentin Boehler, Bradley J. Nelson, and Dario Floreano**

Variable stiffness (VS) is an important feature that significantly enhances the dexterity of magnetic catheters used in minimally invasive surgeries. Existing magnetic catheters with VS consist of sensors, heaters, and tubular structures filled with low melting point alloys, which have a large stiffness change ratio but are toxic to humans. In this paper, a VS magnetic catheter is described for minimally invasive surgery; the catheter is based on a novel variable stiffness thread (VST), which is made of a conductive shape memory polymer (CSMP). The CSMP is nontoxic and simultaneously serves as a heater, a temperature sensor, and a VS substrate. The VST is made through a new scalable fabrication process, which consists of a dipping technique that enables the fabrication of threads with the desired electrical resistance and thickness (with a step size of 70 µm). Selective bending of a multisegmented VST catheter with a diameter of 2.0 mm under an external magnetic field of 20 mT is demonstrated. Compared to existing proof-of-concept VS catheters for cardiac ablation, each integrated VST segment has the lowest wall thickness of 0.75 mm and an outer diameter of 2.0 mm. The segment bends up to 51° and exhibits a stiffness change factor of 21.

1. Introduction

Minimally invasive surgeries provide a lower risk and faster recovery time than conventional procedures since they are used to operate in targeted local regions to curtail the damage caused to healthy tissue. These procedures are increasingly being used to treat conditions such as cardiovascular diseases and cancer.[1–3] Modern medical tools such as catheters are widely used in these surgeries.[3–5] The surgeon inserts a catheter through a well-defined passage in the body to perform the necessary operation.[6] An example of such an operation is the treatment of cardiac arrhythmias by radiofrequency ablation, in which the catheter passes through the right atrium of the heart.[7]

Some conventional catheters used in these surgeries make use of tendon-driven actuation for navigation within the human body.[8] An alternative approach involves the use of remote magnetic catheter navigation. In this case, a permanent magnet is embedded in the catheter, and its motion within the body is controlled by an externally generated magnetic field.[9] This eliminates the need to place actuation mechanisms within the catheter, thereby simplifying the design while still enabling effective navigation to a defined zone during surgery.[10] Moreover, it has been shown that remote magnetic navigation can be learned quickly and that surgeons become adept at using the technology with minimal training.[9] Existing clinical magnetic catheters consist of an ablation tip, a flexible shaft with a working channel, and a given number of permanent magnets that determine the maximum curvature of the catheter under an applied external magnetic field.[10] In the scenario that involves employing a catheter to treat heart arrhythmias by cardiac ablation, it is challenging to keep the catheter tip in contact with the atrial wall to achieve ablation.[6,9,11–13] The complex anatomy of the human heart and lack of 3D visualization require catheters with high dexterity to reach more inaccessible regions.[14–16] Often, surgical procedures, such as those in the heart, require bending catheters in a wide variety of directions to position the tool appropriately. However, the externally generated magnetic field in a remote navigation system is typically confined to a single direction.[17]

To address this problem, researchers have suggested the use of segmented catheters in which individual segments can undergo changes in stiffness and locally resist the magnetic field.

Y. Piskarev, D. Floreano
Laboratory of Intelligent Systems
Institute of Mechanical Engineering
School of Engineering
École Polytechnique Fédérale de Lausanne
Lausanne 1015, Switzerland
E-mail: dario.floreano@epfl.ch

J. Shintake
Shintake Research Group
School of Informatics and Engineering
The University of Electro-Communications
1-5-1 Chofugaoka, Chofu, Tokyo 182-8585, Japan

C. Chautems, J. Lussi, Q. Boehler, B. J. Nelson
Multi-Scale Robotics Lab
Tannenstrasse 3
ETH Zurich
Zurich 8092, Switzerland

The ORCID identification number(s) for the author(s) of this article can be found under https://doi.org/10.1002/adfm.202107662.

DOI: 10.1002/adfm.202107662

This has resulted in an increase in the number of controllable bending directions (degrees of freedom).[6,11,13] Researchers have already presented variable stiffness (VS) catheter phase-change materials (alloys[13] and polymers[18]), hydraulic pressure-driven systems with an array of valves,[19] fiber jamming,[20] granular jamming,[21] and layer jamming.[22]

Hydraulic and jamming technologies show faster reaction times (less than a second) than phase-change materials (seconds to hundreds of seconds);[18,21] however, additional air channels, layers, or granules inside the devices limit miniaturization. Existing hydraulic and jamming-based catheters with diameters of 3.0 and 5.0 mm exceeds the standard diameter of cardiac catheters (2.3 mm) and cannot be used for cardiac ablation.[19,21]

The development of catheters has overcome the scaling problem with the use of low melting point alloys. These materials have a large stiffness change ratio (>400 times) but are toxic and require encapsulation.[6,11,23,24] Moreover, the integration of additional electrical components, such as temperature sensors and heaters (needed to control the stiffness change), leads to a laborious fabrication process. This process has to be adapted for each particular catheter size by developing a new mold made of polydimethylsiloxane (PDMS) or two silicone tubes.[6,11,24] This independent integration of a large number of components also leads to a complicated design and fabrication process that results in a lack of versatility, making it difficult to match the catheter to a given specification for the application.

Here, we present a novel variable stiffness thread (VST) made of a conductive shape memory polymer (CSMP), which is a nontoxic material that simultaneously serves as a heater, a temperature sensor, and a VS substrate.

Shape memory polymers (SMPs) exhibit stiffness changes during the phase transition as well as actuation due to the shape memory effect.[25,26] The stiffness of SMPs can be tuned by varying the temperature above the glass transition temperature with the application of an external stimulus, such as photothermal or Joule heating.[27] When the polymer is heated above the glass transition temperature, it transitions from the solid state with a high load resistance to a rubbery elastic state exhibiting easy deformation. After this transition, a stiffness change amounting to several hundred times the elastic modulus is observed.[28] If the SMP does not undergo large deformations, then the shape memory effect is not dominant, and the heating or cooling of the material changes only the elastic modulus.[26] Among similar materials, polyurethane-based SMPs present several advantages, including easy processing, biocompatibility, an adjustable shape-recovery temperature, and large strain recoveries.[29–31] Thus, they are widely used in soft robotics applications such as variable stiffness actuators, microfluidic valves, and flexible skins.[27,32,33] The inclusion of conductive particles in SMPs enables direct Joule heating by applying a voltage difference to the material without additional heaters.[34]

The VST developed in this study is composed of three layers: a polytetrafluoroethylene (PTFE) tube with a working channel, a CSMP coating, and an encapsulation layer of silicone rubber (**Figure 1**a). The temperature of the CSMP layer increases from room temperature (23 °C) to 80 °C in 36 s via direct Joule heating with an applied power of 1.5 W and in 18 s with 2 W (Figure 1b). When the applied power is turned off, it takes 90 s to return to room temperature (Figure 1c, see Video S1, Supporting Information). The VST with a weight of 0.2 g withstands an applied load of 30 g in the rigid state and exhibits a large deformation in the soft state at 80 °C (Figure 1d, see Video S2, Supporting Information). The thread exhibits a stiffness change factor (SCF) of 21 when heated beyond the glass transition temperature of 45 °C.[34] VSTs are made with a new fabrication method consisting of a dipping technique that enables the fabrication of threads with the desired thickness and electrical resistance. In contrast to conventional tubular VS technologies fabricated through molding or injection processes,[6,23,35] our approach allows VST thickness tuning with a step size of 70 μm.

We validated this method through the characterization of VSTs and then demonstrated the selective bending of a multisegment catheter (Figure 1a). The catheter has an external diameter of 2.0 mm and an internal diameter (i.e., working channel) of 0.5 mm, resulting in a wall thickness of 0.75 mm, which is lower than the thicknesses of other VS cardiac catheters.[6,11] In the VST catheter, each segment bends up to 51° under an 80 mT external magnetic field and has a surface temperature of 41.5 °C. The working channel inside the VST can be used for the incorporation of an active cooling system to enhance the reaction time and provide information flow via the deployment of wires or insertion of surgical tools.

2. Results and Discussion

2.1. Fabrication Method

The VST fabrication procedure based on the dipping technique is illustrated in **Figure 2**. In this method, a PTFE tube fixed on a metal rod is dipped vertically into the CSMP mixture and then cured in an oven, inducing the formation of a CSMP layer on the tube (Figure 2a–c). This dipping step can be repeated multiple times to achieve the desired thickness of the CSMP layer. Then, the tube with the CSMP coating is dipped into liquid silicone and cured in an oven for the purpose of encapsulation (Figure 2d–f). Silicone was chosen as the encapsulation material due to its low thermal conductivity (on the order of 0.2 W m^{-1} K^{-1}) and high electrical breakdown strength (on the order of 53 V μm^{-1}).[36,37] While the dipping technique itself has been widely used in industry due to its high precision control of deposit thickness,[38,39] this is the first time it has been used for coating PTFE tubes with CSMP. In previous work, the CSMP mixture was deposited only on planar surfaces.[34] Therefore, we first assessed how the number of dips affected the thickness of the CSMP layer and its resistance. As shown in **Figure 3**a, the thickness of the CSMP layer increased from 84 to 570 μm from the first to the eighth dip, with a step size of 70 μm. The data show linear behavior, suggesting that the thickness is highly controllable. For the resistance of the CSMP layer, the result shows a quadratic drop. This is because the resistance is inversely proportional to the cross-sectional CSMP area. A significant decrease in the resistance of the VST was observed after the first dip, from 891 ohms down to 374 ohms after the second dip; it ended at 96 ohms after the eighth dip at room temperature.

During the fabrication of VSTs, the CSMP coating on the PTFE tube formed four zones: a wetting zone at the top of the tube, a constant thickness zone, a dynamic meniscus, and a static meniscus.[40] The mixture's wettability (i.e., to what extent

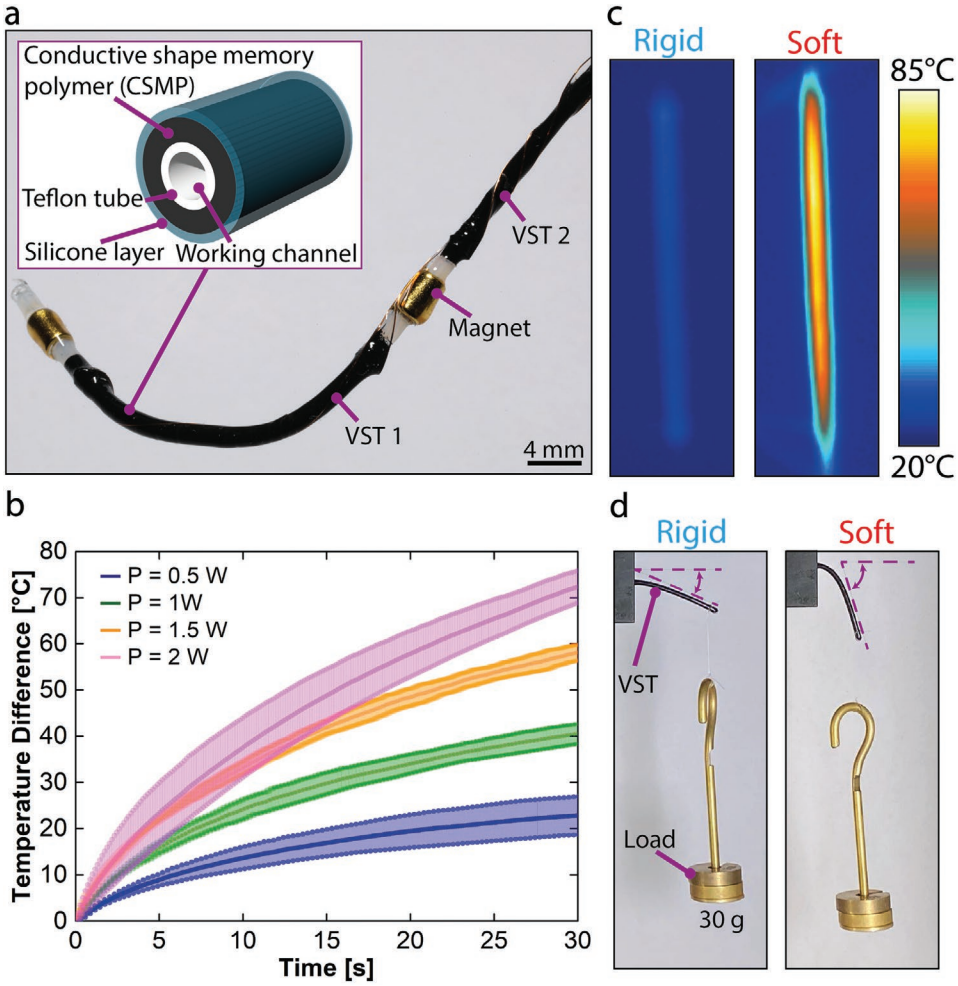

Figure 1. Structure and operating principle of the variable stiffness thread (VST). a) The VST consists of a polytetrafluoroethylene (PTFE) tube with a working channel coated in a conductive shape memory polymer (CSMP) layer, which is further encapsulated in silicone. b) Heating rate of the VST from room temperature (23 °C) for different applied powers. Voltages 7.6, 10.7, 13.1, and 15.1 V were applied to achieve powers of 0.5, 1, 1.5, and 2 W, respectively. Three different samples were tested for each level of applied power. c) The VST can exhibit a change in the stiffness upon direct Joule heating of the CSMP layer. The device undergoes the state change from a rigid state at room temperature (23 °C) to a soft state at 80 °C in 27 s with an applied power of 1.5 W. d) The VST only minimally bends under a weight of 30 g in the rigid state, but freely bends under the same weight when heated to 80 °C in the soft state.

the material spreads across a substrate) is required in order to obtain uniform coating. Wettability depends on the surface tension of the liquid and on the surface energy of the substrate. On the one hand, the high surface tension of the mixture leads to a strong attraction between molecules, resulting in dewetting (i.e., the rupture of a thin liquid film on a substrate and the formation of droplets). On the other hand, the high surface energy generates a greater affinity of the molecules of the mixture toward the substrate, resulting in wetting. Thus, the low surface energy of the substrate or high surface tension of the mixture can result in insufficient coating of the substrate. It is therefore essential to choose a solvent with a lower surface tension than this mixture or by changing the substrate material to one with a higher surface energy.

Existing studies have already described some of the relationships in the dipping technique. The thickness of a layer increases with a longer dipping time.[38] Additionally, the temperature of a rod dipping into the mixture influences the thickness of a coating.[41] A higher temperature for the tool leads to a thicker coating. Furthermore, an increase in viscosity results in the growth of the deposit.[42]

The base material for our VSTs was a cytocompatible polyurethane-based SMP (SMP Technologies Inc., MM4520).[48,49] SMPs are widely used in biomedical applications such as stents, drug delivery, and bone tissue engineering.[29,46,47] PDMS (Dow Corning, Sylgard 184) was applied as an outer coating on the VST due to its biocompatibility with human tissue.[43–45] Carbon black (Nouryon, Ketjenblack EC-600JD), a type of conductive nanofiller, was infused with the thermoplastic polyurethane to improve the mechanical and electrical characteristics without losing biocompatibility,[53] although a detailed biocompatibility study was not performed. However, carbon black has already been used for biocompatible strain sensors and flexible bioelectrodes,[50,51] and the one used in this study showed high cell viability (100%) at a concentration of 32.5 µg mL^{-1} during an in vitro cytotoxicity study.[52] Additionally, as there is no evidence

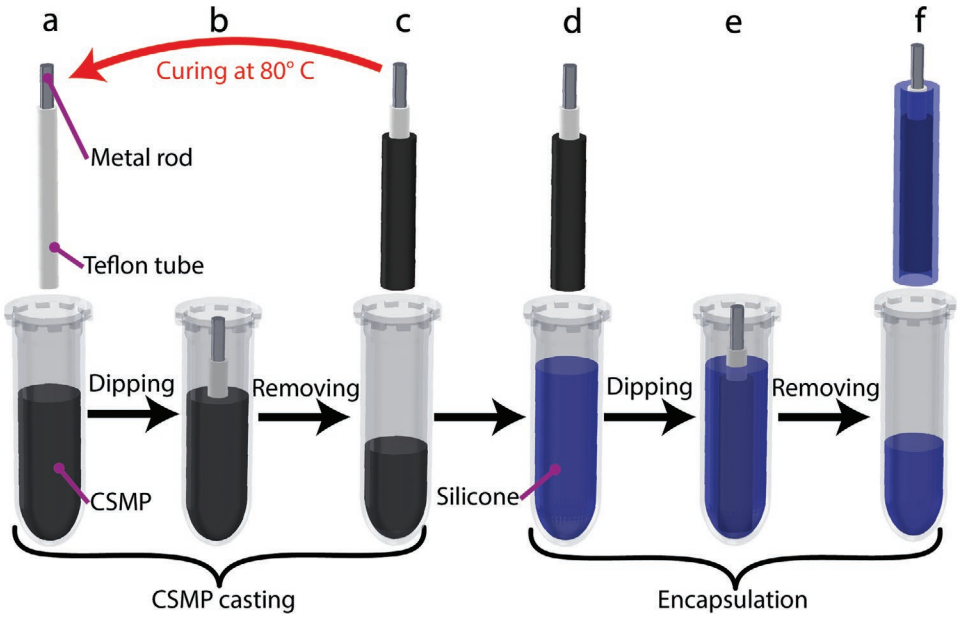

Figure 2. Fabrication process of the variable stiffness threads (VSTs). a) A PTFE tube is prepared and fixed on a metal rod. b) The tube is dipped into a conductive shape memory polymer (CSMP) mixture. c) The tube is hung vertically and cured in an oven. Steps (a–c) can be repeated to achieve the desired thickness of the CSMP layer. d–f) The sample is then dipped into liquid silicone, hung vertically, and cured in an oven, forming an encapsulation layer.

that the CSMP composite is nontoxic, an in vitro cytotoxicity test was performed (according to ISO 10993–5:2009 Biological Evaluation of Medical Devices – Part 5). The results showed the cytocompatibility of the material for at least 284 min, the maximum time duration of a cardiac ablation procedure (Document S1, Supporting Information).[54]

2.2. Electromechanical Characterization of the VST

To quantify the VST electromechanical properties, we characterized the SCF and resistance change at different temperatures. The SCF depends on the geometrical parameters (length and moment of inertia) and material composition of the device. The SCF is given by the relation

$$\mathrm{SCF} = \frac{K_\mathrm{r}}{K_\mathrm{s}} \tag{1}$$

where K_r and K_s are the bending stiffnesses of the VST in the rigid and soft states, respectively.[55,56] The effective bending stiffness of the thread, K, is defined by the relation

$$K = \sum E_\mathrm{avg} I_i \tag{2}$$

where E_avg is the Young's modulus of the entire device. I_i is the moment of inertia (second moment of area) of different layers from i equal to 0 to N. The moment of inertia is determined by the different layers making up the VST: the PTFE, CSMP, and silicone layer. The moment of inertia is given as

$$I_i = \frac{\pi r_\mathrm{e}^4}{4}\left\{1 - \left(\frac{d_\mathrm{i}}{d_\mathrm{e}}\right)^4\right\} \tag{3}$$

where r_e is the external radius, d_i is the internal diameter, and d_e is the external diameter of the layer. To calculate the Young's modulus E_avg, we employ the equation described in ref. [24].

$$E_\mathrm{avg} = \frac{E_\mathrm{PTFE} A_\mathrm{PTFE} + E_\mathrm{CSMP} A_\mathrm{CSMP} + E_\mathrm{silicone} A_\mathrm{silicone}}{A} \tag{4}$$

where A_PTFE, A_CSMP, A_silicone, and A are the cross-sectional areas of the PTFE, CSMP, silicone, and VST, respectively. Similarly, E_PTFE, E_CSMP, and E_silicone are the Young's moduli of PTFE, CSMP, and silicone, respectively. In these parameters, E_CSMP remains uncertain due to the addition of carbon particles.[34] Thus, a thermomechanical characterization of the VST and an empirical study of the bending stiffness were performed. Dynamic mechanical analysis showed a 20-fold reduction in the elastic modulus from 2 to 0.1 GPa as the temperature increased from 37 to 80 °C (Figure S1, Supporting Information). Additionally, the infusion of carbon particles with the thermoplastic polyurethane resulted in a fourfold reduction in the storage and loss moduli of the SMP as the temperature increased from 20 to 120 °C.[27] The carbon particles also shifted the glass transition temperature closer to the temperature of a human body from 60 to 45 °C. The bending stiffness was empirically defined through a three-point flexural test, where the VST was placed in a universal testing machine equipped with a temperature box. The test was conducted at four temperatures: 22 °C for the rigid state and 40, 60, and 80 °C for the soft states. With this experimental condition, the deflection and reaction force of the VST were measured. The results were filtered (see Figure S4, Supporting Information) and plotted in Figure 3b. According to the Euler–Bernoulli beam theory and considering the boundary conditions, the deflection of the VST is expressed as

$$\delta = \frac{Fl^3}{48EI} \tag{5}$$

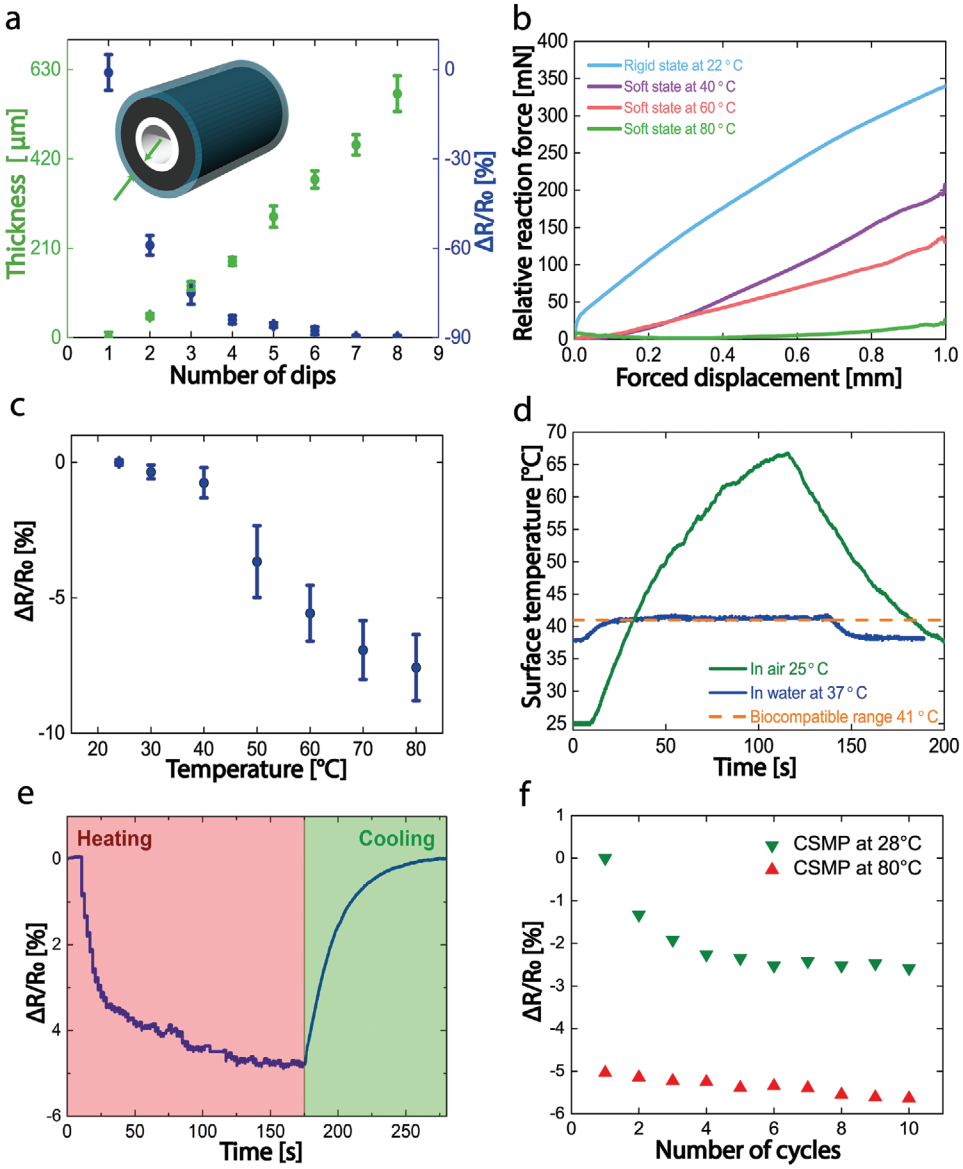

Figure 3. Variable stiffness thread (VST) characterization. The coating thickness of the VSTs was 0.3 mm. a) Thickness and electrical resistance of the conductive shape memory polymer (CSMP) layer as functions of the number of dips. The thickness changes from 84 µm after the first dip to 550 µm after the eighth dip. The resistance decreases from 891 ohms for the first dip to 91 ohms after the eights dip. b) Reaction force of the VST against forced displacement under a three-point flexural test. c) Electrical resistance of the CSMP layer as a function of the temperature change under indirect Joule heating. The resistance decreases from 115.3 ohms at 23 °C to 106.6 ohms at 80 °C, with a significant drop in the range between 23 and 45 °C due to the change in state from solid to rubbery. d) VST with the CSMP layer heated to 80 °C, reaching a surface temperature of 66 °C in air and 41.5 °C in water at 37 °C without flow. e) The state of the VST can be seen with the resistance drop caused by the temperature difference for the cold and hot states. Direct Joule heating under 1 W of applied power increases the VST temperature from room temperature (23 °C) to 80 °C in 175 s in air. Then, the thread cools back down to room temperature in 107 s. During this heating–cooling cycle, the VST experiences a relative resistance change equal to 5%. f) Resistance change in the VST for 10 heating–cooling cycles under direct Joule heating. The green and red triangles represent the resistance change in the rigid state at 28 °C and soft state at 80 °C, respectively. After passing the first three cycles, the resistance change remains almost constant.

where δ is the deflection of the VST at the point of applied force F, l is the length of the beam, E is Young's modulus, and I is the moment of inertia. The multiplication of two parameters EI represents the bending stiffness K of the device. Based on the experimental results and Equation (5), the SCFs of the VST between room temperature (22 °C) and 40, 60, and 80 °C were found to be 1.4, 2.4, and 21, respectively. The corresponding SCF can be defined for specific applied loads in rigid and soft states using Equations (1–5). The coating thickness of the VSTs in all experiments was 0.3 mm.

To characterize the resistance change, six samples were connected to a multimeter, placed in an oven, and heated from 22 °C to 80 °C with a step size of 10 °C. As shown in Figure 3c, the VST experiences a decrease in the resistance

from 115.3 ohms at 23 °C to 106.6 ohms at 80°, resulting in a change of 7.6%. It also shows a significant drop in the temperature range between 23 and 60 °C. The reduction in resistance is due to the negative temperature coefficient, which occurs when the carbon black particles are small and the concentration is near the percolation threshold.[57–60] This effect arises from particle realignment, thermal emission of electrons between nearest carbon black particles, and oxidative crosslinking at the surface.[57,60] Overall, the VST exhibits good sensitivity to temperature changes. This means that the temperature control of the VST can be achieved based on its own resistance change without the use of additional sensing elements and associated electric components.

The VST can be heated with direct Joule heating by applying electrical power to the CSMP layer. The resistance of the device changes as it was heated in the air from 23 to 80 °C in 175 s with an applied power of 1 W (Figure 3e). The VST can be heated to 80 °C in 27 s with an applied power of 1.5 W, which reduces to 18 s with 2 W (Figure 1b). Then, it was cooled back to the initial temperature in 107 s. The result shows a drop of 5% between the rigid and soft states. This resistance drop can be used to sense the current stiffness of the VST. In comparison with an observed resistance drop caused by heating, the resistance change during mechanical deformation is negligible (see Figure S2, Supporting Information). The maximum resistance change under direct heating is 2.6% lower than that in the case of indirect heating (Figure 3c). This can be explained by the inhomogeneous heat distribution in the CSMP material due to variations in the dipping deposit thickness of the CSMP layers. Different thicknesses of the CSMP layer result in local resistance differences between the top, bottom, and middle regions of the VST (Figure 1b).

Regions with higher resistance generate more heat; thus, the temperature is higher in these regions, which leads to a higher resistance difference. As shown in Figure 1b, the temperature of the CSMP layer varies from 80 °C in the middle to 50 °C close to the top and bottom regions of the VST during direct Joule heating. Thus, the temperatures of the CSMP regions at the top and bottom are lower and cause less resistance change difference than in the middle. In contrast, for the case of indirect heating, the VST was homogeneously heated in the oven. The VST heating time from 28 to 80 °C is six times longer for 1 W than for 1.5 W (Figure 1b) due to the lower applied power. During the cyclic thermal loading test, the resistance showed a significant drop after the first three cycles (Figure 3f). This effect is typical for conductive polymers and occurs due to the irreversible change in carbon black aggregation during heating.[57] This aggregation becomes stabilized after the first few cycles and does not return to the initial state after cooling. After passing the first three cycles, the resistance change remains almost invariant for the following seven cycles.

To determine the maximum safe temperature of the CSMP layer in the soft state, we characterized the surface temperature in air at room temperature (23 °C) and in water at 37 °C without forced flow. The temperature of the water was set to mimic the thermal behavior of a VST inside the human body due to its similar heat-transfer properties.[11] Three thermistors were glued on the surface of the VST, covering both ends and the middle. The thermistors were isolated against the water with a layer of glue. The surface temperature was measured by thermistors when heat was applied. The resistance of the CSMP layer was used to define its own temperature during direct Joule heating. First, the CSMP layer was heated to 80 °C in the air with an applied power of 1 W (applied voltage 10.7 V). The temperature was controlled using a thermal camera and by monitoring the resistance change of the CSMP layer. When submerged in water, the applied power was 1.16 W which corresponds to an applied voltage of 12.5 V. The power was turned off when a relative resistance change of 5% was achieved. The result is displayed in Figure 3d. The surface temperature of the VST reached 66 °C in air and 41.5 °C in water when the CSMP layer was heated to 80 °C. The surface temperature in the water was 0.5 °C higher than the required biocompatible surface temperature.[61] This was a result of the fact that the test was conducted in stagnant water. In minimally invasive surgery, the VST will be surrounded by flowing fluid, which will reduce the surface temperature below the safe temperature. A further reduction in surface temperature can be achieved by increasing the thickness of the silicone layer by 65 μm or by modifying the material composition of the insulating layer (see Figure S3, Supporting Information).

2.3. Electromechanical Characterization of a Single-Segment VST Catheter

We assessed the performance of a single segment of a VST catheter in terms of the bending angle in the soft and rigid states under external magnetic fields. The bending angle in the soft state determines the level of dexterity of a catheter. In the VST rigid state, the bending angle defines the magnetic torque the catheter can withstand, thus governing the level of shape fixity that can be achieved. The external magnetic field B applied on a permanent magnet with a dipole moment m at position p generates a magnetic torque T_m

$$T_m(p) = m \times B(p) \tag{6}$$

The maximum magnetic torque is achieved when the magnetic field is perpendicular to the dipole moment and is minimal when they are aligned. On the other hand, the magnetic torque can be tuned by choosing permanent magnets with higher dipole moments.

The design of the single-segment VST catheter is illustrated in **Figure 4**a-i. It consists of a VST attached to a base on one end and is equipped with a permanent magnet on the other. An electrode is connected to one end of the VST and wrapped around and down to the base to deliver power to the CSMP layer. The entire structure is encapsulated in silicone. It has a length of 44 mm, an outer diameter of 2.0 mm, and an internal diameter, that is, the working channel, of 0.5 mm (Figure 4a-ii). This design has the same working channel size but a lower wall thickness of 0.75 mm compared to a previously developed low melting point alloy-based catheter with a wall thickness of 0.92 mm and an outer diameter of 2.3 mm.[11]

The deflection of a single-segmented catheter is characterized inside the electromagnetic navigation system with a magnetic field magnitude of 80 mT and varying magnetic field

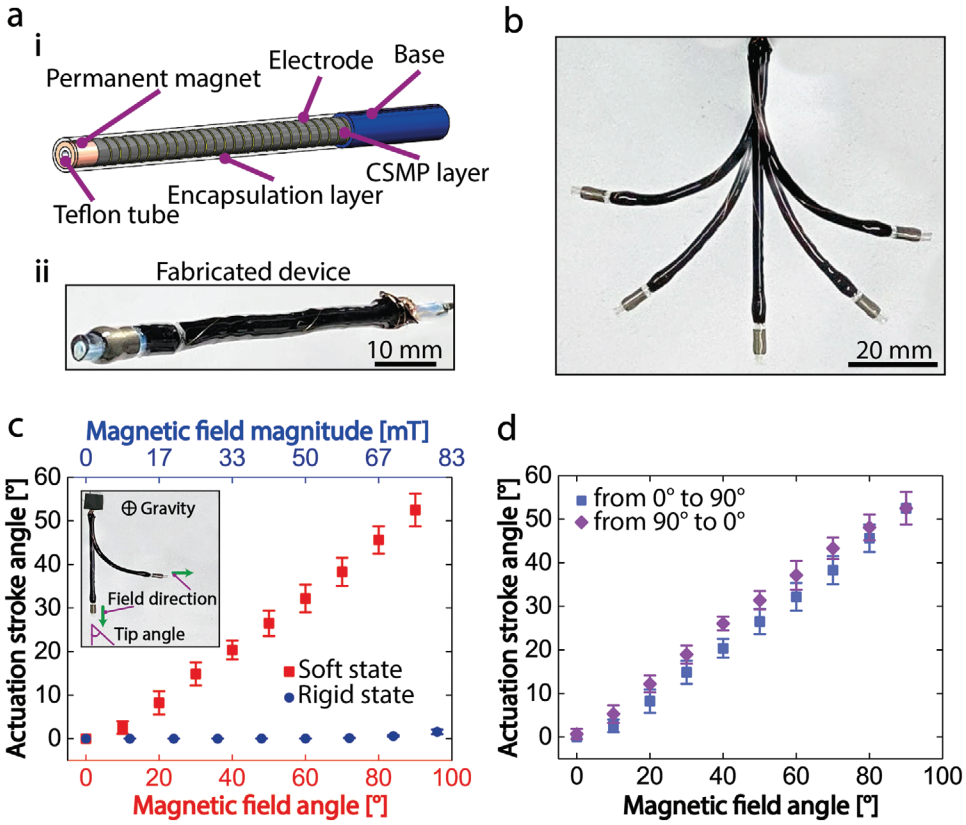

Figure 4. Single-segment catheter with variable stiffness thread (VST) and characterization results. a) i) The catheter consists of a VST, permanent magnet, base part, and electrode wire wrapped around the conductive shape memory polymer (CSMP) layer. The entire structure is encapsulated in silicone. ii) The catheter has a length of 44 mm and a diameter of 2.0 mm with a working channel of 0.5 mm. b) Bending actuation of the VST catheter. c) Actuation stroke angle as a function of the magnetic field angle and magnitude. The values represent three tested catheters and five cycles per device. The maximum actuation angle in the rigid state under a magnetic field magnitude of 80 mT is 1.5°. In the soft state, the actuation angle exhibits the maximum value of 51° under a magnetic field angle of 90°. d) Actuation stroke angle as a function of the magnetic field angle in the soft state. The values represent three tested catheters and five cycles per device.

orientations. The catheter can bend up to 90° in the desired direction in the soft state under 80 mT (Figure 4b). The motion of the device can be observed in Video S3, Supporting Information. The characterization results, plotted in Figure 4c, show that the VST catheter can withstand the applied magnetic moment and bend only up to 1.5° at the maximum magnetic field of 80 mT.

In the soft state, the device exhibits a linear change in the bending angle up to 51° at an inclination angle of 90° and a magnetic flux density of 80 mT. As shown in Figure 4d, the device also demonstrates high repeatability with a low hysteresis for five cycles. Note that the values in Figure 4c,d represent three tested catheters and five cycles per device. Compared with existing models that can bend up to 110°, the maximum bending angle in the current system is 90°.[6,11] In terms of performance repeatability, fatigue was not observed after 10 cycles of testing.[11]

2.4. Multisegmented Catheter for Cardiac Ablation

To better illustrate the possible application of VST, we developed a multisegmented catheter with two integrated VSTs for use in medical scenarios such as cardiac ablation (**Figure 5**). The device consists of two variable stiffness segments with two permanent magnets (Figures 1a and 5a). The VSTs were fabricated separately and mounted on the PTFE tube together with magnets. Then, the whole structure was encapsulated by dipping it into the silicone. Our objective is to demonstrate that a multisegmented catheter composed of two VSTs can be manipulated with a magnetic field as low as 20 mT. Thus, according to Equation (6), the induced magnetic torque for a two-segmented VST catheter is lower than that for a single-segmented catheter, where an external magnetic flux density of 80 mT is applied. Therefore, permanent magnets with a four times higher dipole moment m are selected to provide the same magnetic torque for the two-segmented catheter.

The catheter was first placed in the electromagnetic navigation system with rigid VSTs (Figure 5a-i). Magnetic flux was applied perpendicular to the length of the catheter to generate deflection of the tip in the rigid state (see Video S4, Supporting Information). Then, the VSTs were heated up and bent to realize catheter deflection. As shown in Figure 5a-ii–iv, the selective activation of VSTs enables different deformations of the device. Each of the segments can be bent up to 90°, while the second segment withstands an applied magnetic torque

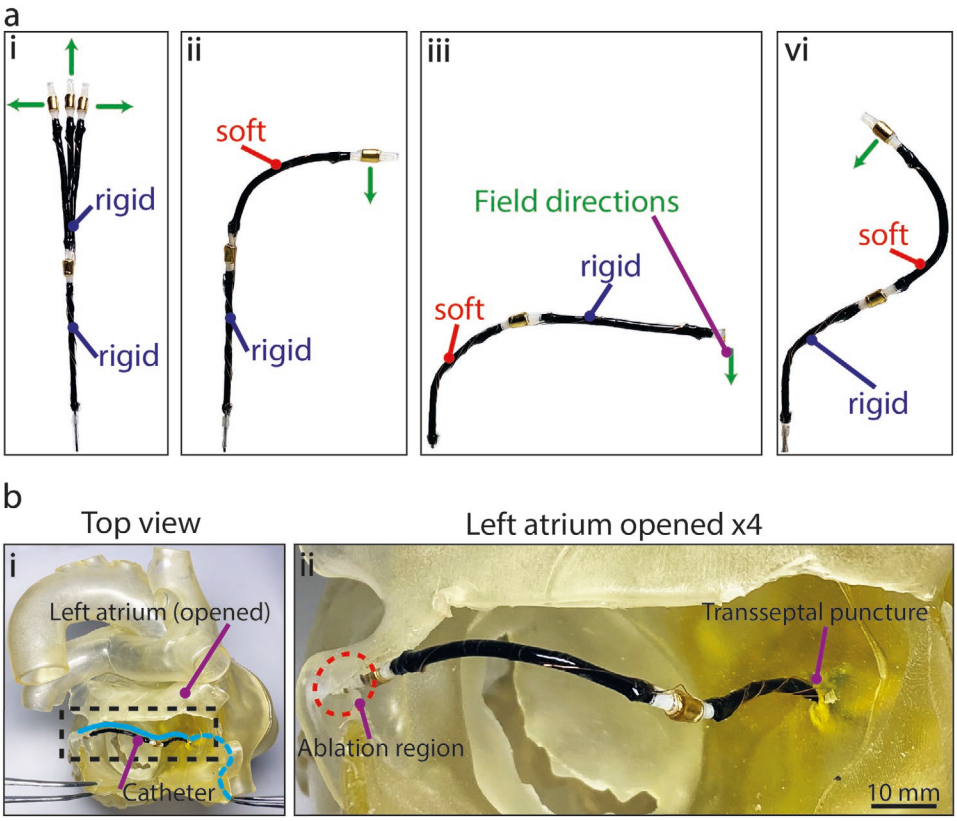

Figure 5. Two-segmented catheter design, performance, and application. a) The catheter consists of two variable stiffness threads (VSTs) and two permanent magnets fastened on the same PTFE tube. The catheter is placed in an electromagnetic navigation system i) when both VSTs are solid and ii–iv) when one of them is sequentially soft. b) An illustration of catheter application in the cardiac ablation procedure. The path of the catheter is shown in blue: it goes through the right femoral vein and inferior vena cava into the right atrium, through which, with a transseptal puncture, it reaches the left atrium. In the left atrium, the catheter reaches one of the four pulmonary veins (i, ii).

(Figure 5a-ii,iii). The catheter achieves complex curvatures by inducing sequential stiffening/destiffening of each VST segment (Figure 5a-iv). Thus, the device is more dexterous than the single-segmented catheter due to additional degrees of freedom obtained with two integrated VSTs. When both VSTs are in a rigid state, the workspace of the catheter consists of rotation in a circular trajectory with a diameter of 8 mm. Reducing the stiffness of the segments increases the workspace by 41 mm when the top VST is heated and by 78 mm when the bottom VST is in the soft state.

To illustrate the medical application, the catheter was inserted into a 3D printed model of a human heart (Figure 5b-i). The device was placed in the final position of the desired path (shown in blue) to reach the ablation region in one of the pulmonary veins (in red). In Figure 5b-i,ii, an example of an ablation location around one of the four pulmonary veins is presented. Monitoring the position of the catheter's tip can be achieved using an X-ray machine to detect a magnet on the tip and electrodes running along the catheter's length.[62]

3. Conclusion

We have described a method for creating tubular variable stiffness devices made of CSMPs, namely, VSTs. Our method relies on a dipping technique, which enables the fabrication of VSTs with the desired thickness and electrical resistance. The CSMP layer in the VST is nontoxic and simultaneously serves as a variable stiffness substrate, heater, and temperature sensor. Using this technique, we developed multisegmented VST catheters with integrated permanent magnets. The device demonstrated stiffness control and selective bending of each segment. Stiffness control is realized thanks to a resistance drop in the CSMP layer of up to 7.6%. In the soft state, each of the VS segments can bend up to 51°. When switched to the rigid state, the catheter can withstand applied magnetic fields up to 80 mT due to the 21× increase in the bending stiffness of VSTs. Our catheter design has the lowest wall thickness of 0.75 mm and outer diameter of 2 mm compared to existing proof-of-concept VS catheters for cardiac ablation.[11]

In addition to their application in very constrained procedures such as cardiac ablation, magnetically driven VS catheters are being used in other procedures in organs such as the stomach, lungs, and brain.[63] The scalable fabrication process of a simple three-layer VST that we presented can easily be adapted to produce catheters with various thicknesses suitable for these applications.

The VST was fabricated using nontoxic materials including PTFE, carbon particles,[30] and polyurethane-based SMP,[29] as well as PDMS, where the latter is biocompatible.[43] However,

the biocompatibility of the VST is not guaranteed by using non-toxic materials in the CSMP layer, and therefore, further testing is required. The VST was therefore investigated in accordance with the International Organization for Standardization (ISO) 10 993 for medical devices, which include tests for factors such as irritation, sensitization, and hemolysis.[64]

The working channel inside the VST can be used for incorporating an active cooling system to enhance the reaction time since this was already presented for variable stiffness soft pneumatic actuators.[65] The VST sensitivity to temperature can be controlled by adapting the quantity of conductive filler.[57] The temperature of the external surface can potentially be decreased by increasing the thickness of the outer silicone layer or changing the isolation material to perfluoropolyether (PFPE), which has lower thermal conductivity and is already used for medical applications.[24] Further interface tests between the VST and human tissue will shed light on the fouling rate and thrombi formation caused by heating of the CSMP layer. Mixing time, speed, and temperature affect the resistivity of a final conductive composite. In addition, the volume resistivity and Mooney viscosity influence the absolute stiffness and thickness of a polymer.[34,57–60] The robustness of the electrical and mechanical properties of CSMPs under thermal and mechanical loadings in intermediate stiffness regimes should also be investigated. The precision of the dipping technique could be improved by decreasing the viscosity of the liquid CSMP mixture. Automation of the fabrication process is another way to enhance precision. The VST could be useful not only in endoscopic devices with different mechanical and geometrical specifications but also in the development of smart fabrics that would require weaving the VSTs into a textile.[23,35,66] The stiffness and size of VSTs used in rehabilitation fabrics can be easily scaled up or down due to the simplicity of the dipping technique. We believe that the capabilities of VSTs enable their use in applications beyond medicine, where the size and weight of the system play a crucial role. Such applications include incorporation into space or flying vehicles to achieve, for example, different locomotion modes.[23]

4. Experimental Section

Fabrication of the Variable Stiffness Thread: The fabrication of VSTs consists of three main steps: preparation of a CSMP mixture, fabrication of CSMP tubes through a dipping technique, and encapsulation of the tube. For the CSMP mixture, commercially available pellets of polyurethane (PU) SMP (MM4520, SMP Technologies) were mixed with a solvent (dimethylformamide, DMF; Sigma-Aldrich) in a weight proportion of 1 to 4 and stirred without heating for 8 h. Then, 1.2 g of carbon black powder (Nouryon, Ketjenblack EC-600JD) and 36 g of DMF were added to 30 g of homogenous SMP mixture. The mixture was then milled together with six metal balls (diameters of 10 mm) where the generated shear forces break down the agglomerations of carbon black powder and disperse it homogeneously in the polymeric matrix.[67–69] A PTFE tube with an inner diameter of 0.5 mm and an outer diameter of 0.9 mm was dipped vertically in an already-prepared conductive mixture. Thereafter, the tube was hung vertically and cured in an oven at 80 °C for an hour. The dipping process was repeated five times to obtain a 300 µm thickness of the CSMP layer used in the VST catheter. After completing the five dips, the samples were cured in an oven at 80 °C for 8 h to evaporate the remaining solvent. Finally, the manufactured tube was vertically dipped in liquid PDMS (Dow Corning, Sylgard 184) and cured in an oven for 30 min.

Reaction Force Measurement: A three-point flexural test was used to determine the SCF of the VSTs, which were placed in a universal testing machine (Instron 5965) equipped with a temperature control box. The testing machine was equipped with 3D printed acrylonitrile butadiene styrene (ABS) support parts and a rail manufactured based on the standard ISO178:2019, which defines the conditions for three-point flexural tests on universal testing systems. The tests were conducted at four temperatures of 23 °C (room temperature) for the rigid state and 40, 60, and 80 °C for the soft state to collect the deflection and reaction force of the VST. The raw data of reaction force against forced displacement were filtered using the infinite impulse response (IIR) filtering tool in Origin Pro 2016. A Butterworth filter with a pass frequency of 10 Hz was applied.

Heating and Cooling Times Characterization: Temperature readings were sampled using a thermal camera (FLIR, E8xt) that was placed 100 mm from the VST. Three samples were collected for each of the four applied voltages 7.6, 10.7, 13.1, and 15.1 V, which resulted in the applied powers of 0.5, 1, 1.5, and 2 W, respectively. The VST was cooled to room temperature between each measurement and the heating profile of the VST was processed using FLIR ResearchIR Software.

Resistance Change Measurement: The VST was heated using direct Joule heat generated by a power supply (BK Precision, 9141) with a constant applied voltage. The resistance change of the VST was measured using an electric circuit consisting of a power supply, a resistor of 2.2 kohm, and the VST connected in series. In parallel to the VST, two resistors of 8 and 4 kohm were connected. The voltage on the resistor of 4 kohm was red using a digit multimeter (BK Precision, 5493C).

Cyclic Thermal Loading Measurement: The temperature of the VST was monitored with a thermal camera (FLIR, T911098) when heated through a power supply (BK Precision, 9141). The resistance was measured with a digit multimeter (BK Precision, 5493C).

Surface Temperature Measurement: The surface temperature was measured by placing TDK thermistors on the outer silicone layer of the VST while the temperature was increased via direct Joule heating. The VST was heated by applying 10.7 V with a power supply (BK Precision, 9141) when in air and 12.5 V when in water. Each of the applied powers resulted in a relative resistance change of 5% in the CSMP layer. The thermistor data were collected with multifunction data acquisition hardware (LabJack, U3-HV).

Actuation Stroke Angle Measurement: The one-segment catheter was placed in the working area of the remote magnetic navigation system CardioMag and was mounted with a holder screw to the bottom of the working area. The catheter in the rigid state was placed with the magnetic field orientation perpendicular to the permanent magnet field attitude to maximize the bending moment of the permanent magnet. At the same time, the device was placed parallel to the ground to prevent a gravitational effect on the bending performance. The catheter was deflected under an external magnetic field with a flux density from 20 to 80 mT. The magnetic field density and direction were controlled by regulating the currents in each of the eight electromagnets, which were placed in a hemispheric arrangement. We used three cameras and image processing in MATLAB to determine the tip angle deflection of the devices and characterize the actuation stroke angle during multiple cyclic tests.

Supporting Information

Supporting Information is available from the Wiley Online Library or from the author.

Acknowledgements

The authors thank William Stewart and Krishna Manaswi Digumarti for their help with the manuscript and "UFAG LABORATORIEN" for their

support with the cytotoxicity experiments. This work was supported by the SNSF Bridge project 20B2-1 180861 and JSPS KAKENHI Grant-in-Aid for Scientific Research on Innovative Areas "Science of Soft Robot" project (grant number 21H00324).

Open access funding provided by Ecole Polytechnique Federale de Lausanne.

Conflict of Interest

The authors declare no conflict of interest.

Data Availability Statement

The data that support the findings of this study are available on request from the corresponding author. The data are not publicly available due to privacy or ethical restrictions.

Keywords

conductive shape memory polymers, continuum robots, magnetic navigation, medical robotics, multifunctionality, soft robotics, variable stiffness

Received: August 4, 2021
Revised: December 13, 2021
Published online:

[1] E. Bacha, D. Kalfa, *Nat. Rev. Cardiol.* **2014**, *11*, 24.
[2] S. S. A. Y. Biere, M. I. van Berge Henegouwen, K. W. Maas, L. Bonavina, C. Rosman, J. R. Garcia, S. S. Gisbertz, J. H. G. Klinkenbijl, M. W. Hollmann, E. S. M. de Lange, H. J. Bonjer, D. L. van der Peet, M. A. Cuesta, *Lancet* **2012**, *379*, 1887.
[3] M. Han, L. Chen, K. Aras, C. Liang, X. Chen, H. Zhao, K. Li, N. R. Faye, B. Sun, J.-H. Kim, W. Bai, Q. Yang, Y. Ma, W. Lu, E. Song, J. M. Baek, Y. Lee, C. Liu, J. B. Model, G. Yang, R. Ghaffari, Y. Huang, I. R. Efimov, J. A. Rogers, *Nat. Biomed. Eng.* **2020**, *4*, 997.
[4] T. P. Martens, A. F. G. Godier, J. J. Parks, L. Q. Wan, M. S. Koeckert, G. M. Eng, B. I. Hudson, W. Sherman, G. Vunjak-Novakovic, *Cell Transplant.* **2009**, *18*, 297.
[5] T. J. Oxley, N. L. Opie, S. E. John, G. S. Rind, S. M. Ronayne, T. L. Wheeler, J. W. Judy, A. J. McDonald, A. Dornom, T. J. H. Lovell, C. Steward, D. J. Garrett, B. A. Moffat, E. H. Lui, N. Yassi, B. C. V. Campbell, Y. T. Wong, K. E. Fox, E. S. Nurse, I. E. Bennett, S. H. Bauquier, K. A. Liyanage, N. R. van der Nagel, P. Perucca, A. Ahnood, K. P. Gill, B. Yan, L. Churilov, C. R. French, P. M. Desmond, et al., *Nat. Biotechnol.* **2016**, *34*, 320.
[6] C. Chautems, A. Tonazzini, D. Floreano, B. J. Nelson, *IROS*, IEEE, New Jersey **2017**, pp. 181–186.
[7] M. El Baba, D. Sabayon, M. M. Refaat, *J. Innov. Card. Rhythm Manag.* **2020**, *11*, 4234.
[8] Z. Li, L. Wu, H. Ren, H. Yu, *Mech. Mach. Theory* **2017**, *107*, 148.
[9] C. Pappone, G. Vicedomini, F. Manguso, F. Gugliotta, P. Mazzone, S. Gulletta, N. Sora, S. Sala, A. Marzi, G. Augello, L. Livolsi, A. Santagostino, V. Santinelli, *J. Am. Coll. Cardiol.* **2006**, *47*, 1390.
[10] E. S. Gang, B. L. Nguyen, Y. Shachar, L. Farkas, L. Farkas, B. Marx, D. Johnson, M. C. Fishbein, C. Gaudio, S. J. Kim, *Circ. Arrhythm. Electrophysiol.* **2011**, *4*, 770.
[11] C. Chautems, A. Tonazzini, Q. Boehler, S. Jeong, D. Floreano, B. Nelson, *Adv. Intell. Syst.* **2020**, *2*, 1900086.
[12] J. K.-R. Chun, S. Ernst, S. Matthews, B. Schmidt, D. Bansch, S. Boczor, A. Ujeyl, M. Antz, F. Ouyang, K.-H. Kuck, *Eur. Heart J.* **2007**, *28*, 190.
[13] R. Zhao, Y. Yao, Y. Luo, *J. Med. Devices* **2016**, *10*, 021002.
[14] C. Piorkowski, C. Eitel, S. Rolf, K. Bode, P. Sommer, T. Gaspar, S. Kircher, U. Wetzel, A. S. Parwani, L.-H. Boldt, M. Mende, A. Bollmann, D. Husser, N. Dagres, M. Esato, A. Arya, W. Haverkamp, G. Hindricks, *Circ. Arrhythm. Electrophysiol.* **2011**, *4*, 157.
[15] P. Kanagaratnam, M. Koa-Wing, D. T. Wallace, A. S. Goldenberg, N. S. Peters, D. W. Davies, *J. Interv. Card. Electrophysiol.* **2008**, *21*, 19.
[16] L. Mantziari, I. Suman-Horduna, M. Gujic, D. G. Jones, T. Wong, V. Markides, J. P. Foran, S. Ernst, *Pacing Clin. Electrophysiol. PACE* **2013**, *36*, 757.
[17] J. Rahmer, C. Stehning, B. Gleich, *Sci. Robot.* **2017**, *2*, eaal2845.
[18] H. Dong, G. M. Walker, *Smart Mater. Struct.* **2012**, *21*, 042001.
[19] K. Ikuta, H. Ichikawa, K. Suzuki, D. Yajima, in *Proc. Int. Conf. Robotics and Automation, ICRA 2006*, IEEE, New Jersey **2006**, pp. 4161–4166.
[20] M. Brancadoro, M. Manti, F. Grani, S. Tognarelli, A. Menciassi, M. Cianchetti, *Front. Robot. AI* **2019**, *6*, 12.
[21] M. Cianchetti, T. Ranzani, G. Gerboni, T. Nanayakkara, K. Althoefer, P. Dasgupta, A. Menciassi, *Soft Robot.* **2014**, *1*, 122.
[22] Y.-J. Kim, S. Cheng, S. Kim, K. Iagnemma, *IEEE Trans. Robot.* **2013**, *29*, 1031.
[23] A. Tonazzini, S. Mintchev, B. Schubert, B. Mazzolai, J. Shintake, D. Floreano, *Adv. Mater.* **2016**, *28*, 10142.
[24] J. Lussi, M. Mattmann, S. Sevim, F. Grigis, C. De Marco, C. Chautems, S. Pané Vidal, J. Puigmartí-Luis, Q. Boehler, B. Nelson, *Adv. Sci.* **2021**, *8*.
[25] Q. Yang, J. Fan, G. Li, *Appl. Phys. Lett.* **2016**, *109*, 183701.
[26] M. Manti, V. Cacucciolo, M. Cianchetti, *IEEE Robot. Autom. Mag.* **2016**, *23*, 93.
[27] B. Aksoy, H. Shea, *Adv. Funct. Mater.* **2020**, *30*, 2001597.
[28] K. Takashima, K. Sugitani, N. Morimoto, S. Sakaguchi, T. Noritsugu, T. Mukai, *Smart Mater. Struct.* **2014**, *23*, 125005.
[29] J. Delaey, P. Dubruel, S. Van Vlierberghe, *Adv. Funct. Mat.* **2020**, *30*, 1909047.
[30] I. Rajzer, E. Menaszek, L. Bacakova, M. Rom, M. Blazewicz, *J. Mater. Sci. Mater. Med.* **2010**, *21*, 2611.
[31] A. Firouzeh, M. Salerno, J. Paik, *IEEE Trans. Robot.* **2017**, *33*, 765.
[32] B. Aksoy, N. Besse, R. J. Boom, B.-J. Hoogenberg, M. Blom, H. Shea, *Lab Chip* **2019**, *19*, 608.
[33] N. Besse, S. Rosset, J. J. Zarate, H. Shea, *Adv. Mater. Technol.* **2017**, *2*, 1700102.
[34] D. McCoul, S. Rosset, N. Besse, H. Shea, *Smart Mater. Struct.* **2016**, *26*, 025015.
[35] T. P. Chenal, J. C. Case, J. Paik, R. K. Kramer, *IEEE* **2014**, 2827.
[36] S. Vlassov, S. Oras, M. Timusk, V. Zadin, I. Sosnin, R. Lõhmus, L. M. Dorogin, **2020**.
[37] A. H. A. Razak, A. L. Skov, *RSC Adv.* **2016**, *7*, 468.
[38] R. Groves, A. F. Routh, *J. Polym. Sci., Part B: Polym. Phys.* **2017**, *55*, 1633.
[39] R. B. Arumathanthri, B. S. K. Abeygoonawardana, I. D. C. D. Kumarasinghe, D. S. Chathuranga, T. D. Lalitharatne, A. L. Kulasekera, in *2018 IEEE International Conference on Robotics and Biomimetics (ROBIO)*, IEEE, Kuala Lampur, Malaysia **2018**, pp. 2082–2087.
[40] E. Rio, F. Boulogne, *Adv. Colloid Interface Sci.* **2017**, *247*, 100.
[41] M. Barletta, G. Simone, V. Tagliaferri, *Prog. Org. Coat.* **2005**, *54*, 390.
[42] K. K. Sasidharan, R. Joseph, G. Rajammal, P. V. Pillai, K. S. Gopalakrishnan, *J. Appl. Polym. Sci.* **2001**, *81*, 3141.
[43] S. H. Kim, J.-H. Moon, J. H. Kim, S. M. Jeong, S.-H. Lee, *Biomed. Eng. Lett.* **2011**, *1*, 199.
[44] S.-J. Kim, D.-S. Lee, I.-G. Kim, D.-W. Sohn, J.-Y. Park, B.-K. Choi, S.-W. Kim, *Kaohsiung J. Med. Sci.* **2012**, *28*, 123.

[45] C. Potrich, L. Lunelli, M. Cocuzza, S. L. Marasso, C. F. Pirri, C. Pederzolli, *Talanta* **2019**, *193*, 44.
[46] J. Han, G. Fei, G. Li, H. Xia, *Macromol. Chem. Phys.* **2013**, *214*, 1195.
[47] Y.-J. Wang, U.-S. Jeng, S. Hsu, *ACS Biomater. Sci. Eng.* **2018**, *4*, 1397.
[48] L. de Nardo, S. Bertoldi, A. Cigada, M. C. Tanzi, H. J. Haugen, S. Farè, *J. Appl. Biomater. Funct. Mater.* **2012**, *10*, 119.
[49] K. Pieri, "*4D Printing Shape Memory Polymers for Biomedical Applications*" **2020**, https://surface.syr.edu/etd/1256.
[50] P. Lugoda, J. C. Costa, L. A. Garcia-Garcia, A. Pouryazdan, Z. Jocys, F. Spina, J. Salvage, D. Roggen, N. Münzenrieder, *Adv. Mater. Technol.* **2021**, *6*, 2000780.
[51] M. Buaki-Sogó, L. García-Carmona, M. Gil-Agustí, M. García-Pellicer, A. Quijano-López, *Nanomaterials* **2021**, *11*, 2052.
[52] G. Panomsuwan, C. Chokradjaroen, R. Rujiravanit, T. Ueno, N. Saito, *Jpn. J. Appl. Phys.* **2017**, *57*, 0102BGBG.
[53] N. P. Kim, *Polymers* **2020**, *12*, 1224.
[54] F. Keçe, K. Zeppenfeld, S. A. Trines, *Arrhythmia Electrophysiol. Rev.* **2018**, *7*, 169.
[55] J. Shintake, B. Schubert, S. Rosset, H. Shea, D. Floreano, in *2015 IEEE/RSJ Int. Conf. Intelligent Robots and Systems*, IEEE, New York **2015**, pp. 1097–1102.
[56] E. Piskarev, J. Shintake, V. Ramachandran, N. Baugh, M. D. Dickey, D. Floreano, *Adv. Intell. Syst.* **2020**, *2*, 2000069.
[57] K. P. Sau, T. K. Chaki, D. Khastgir, *J. Appl. Polym. Sci.* **1999**, *71*, 887.
[58] Z.-D. Xiang, T. Chen, Z.-M. Li, X.-C. Bian, *Macromol. Mater. Eng.* **2009**, *294*, 91.
[59] N. C. Das, T. K. Chaki, D. Khastgir, *Carbon* **2002**, *40*, 807.
[60] J. Shintake, E. Piskarev, S. H. Jeong, D. Floreano, *Adv. Mat. Techn.* **2018**, *3*, 1700284.
[61] L. Blanc, A. Delchambre, P. Lambert, **2017**, *6*, 23.
[62] Y. Ma, N. Gogin, P. Cathier, R. J. Housden, G. Gijsbers, M. Cooklin, M. O'Neill, J. Gill, C. A. Rinaldi, R. Razavi, K. S. Rhode, *Med. Phys.* **2013**, *40*, 071902.
[63] A. Loeve, P. Breedveld, J. Dankelman, *IEEE Pulse* **2010**, *1*, 26.
[64] S. Srisang, A. Boongird, M. Ungsurungsie, P. Wanasawas, N. Nasongkla, *J. Biomed. Mater. Res. B Appl. Biomater.* **2021**, *109*, 496.
[65] Y.-F. Zhang, N. Zhang, H. Hingorani, N. Ding, D. Wang, C. Yuan, B. Zhang, G. Gu, Q. Ge, *Adv. Funct. Mat.* **2019**, *29*, 1806698.
[66] T. L. Buckner, R. Kramer-Bottiglio, *Multifunct. Mater.* **2018**, *1*, 012001.
[67] S. Rosset, O. A. Araromi, S. Schlatter, H. R. Shea, *J. Vis. Exp.* **2016**, e53423.
[68] K. Awasthi, R. Kamalakaran, A. K. Singh, O. N. Srivastava, *Int. J. Hydrog. Energy* **2002**, *27*, 425.
[69] C.-K. Leong, D. D. L. Chung, *Carbon* **2003**, *41*, 2459.